Food Hydrocolloids 51 (2015) 432–440

Contents lists available at ScienceDirect

Food Hydrocolloids

journal homepage: www.elsevier.com/locate/foodhyd

Thermoplastic starch/talc bionanocomposites. Influence of particle morphology on final properties

Luciana A. Castillo [a], Olivia V. López [a, b, *], Julia Ghilardi [c], Marcelo A. Villar [a], Silvia E. Barbosa [a], M. Alejandra García [b]

[a] Planta Piloto de Ingeniería Química, PLAPIQUI (UNS-CONICET), Departamento de Ingeniería Química, UNS, Camino La Carrindanga Km. 7, 8000 Bahía Blanca, Argentina
[b] Centro de Investigación y Desarrollo en Criotecnología de Alimentos, CIDCA (UNLP-CONICET), Facultad de Ciencias Exactas, UNLP, 47 y 116, 1900 La Plata, Argentina
[c] Departamento de Ingeniería Química, UNS, Av. Alem 1253, 8000 Bahía Blanca, Argentina

ARTICLE INFO

Article history:
Received 28 August 2014
Received in revised form
7 April 2015
Accepted 23 May 2015
Available online 11 June 2015

Keywords:
Composite films
Thermoplastic corn starch
Talc morphology
Composite films microstructure
Barrier and mechanical properties

ABSTRACT

This work analyzed the effect of talc morphology on structural characteristics and final properties of thermoplastic corn starch (TPS). In this sense, composite films based on TPS containing talc nanoparticles were obtained by melt-mixing and thermo-compression. Talc samples with different morphological characteristics (platy-microcrystalline and blocky-macrocrystalline), derived from their formation process, were used. Platy and blocky morphology was distinguished by Scanning Electron Microscopy performed on composites films. Microcrystalline morphology induced smaller TPS crystallites than macrocrystalline one, indirectly evidenced by X-Ray Diffraction and Differential Scanning Calorimetry. Crystalline character of talc particles also affected visible and UV barrier capacity of TPS films. Blocky morphology of mineral filler led to the highest reduction of TPS water vapor permeation. Both talc samples acted as matrix reinforcement agents. However, macrocrystalline particles induced the major changes on elastic modulus and tensile strength, without affecting films ductility.

1. Introduction

Nowadays, technological interest is focused on a new generation of composites polymers based on biodegradable matrixes from renewable raw materials with organic or mineral fillers. These biocomposites have several advantages mainly due to their eco-friendly character since they can be naturally degraded plus their renewable origin. Moreover, these materials could be developed from residues or sub-products, as well as, resources derived from agro–industrial activities. In this sense, starch qualifies as a good option because of its world-wide availability, low cost, functionality and biodegradability. In order to evaluate biodegradable character of materials based on these polymers, several techniques were studied being composting, one of the most used (Saiah, Gattin, & Sreekumar, 2012). Naturally, starch is not considered as a thermoplastic polymer but its processing, in the presence of plasticizers, under high temperature and shear stresses, allows the disruption of its granular structure, becoming into thermoplastic starch (TPS) (Ma, Chang, Yu, & Stumborg, 2009; Pinto, Carbajal, Wypych, Ramos, & Satyanarayana, 2009). TPS-based materials have received considerable attention since their processing is easily scalable, employing the same technology used for synthetic polymers (Parra, Tadini, Ponce, & Lugão, 2004; Tapia Blácido, Sobral, & Menegalli, 2005). In the literature, there are many works related to starch biocomposites development through the incorporation of natural fibers (Narkchamnan & Sakdaronnarong, 2013), nanocrystals (Bodirlau, Teaca, & Spiridon, 2013; Lu, Weng, & Cao, 2005), and clay minerals (Chung et al., 2010; De Melo et al., 2011), among others. Mineral filler presence allows tailoring composites for specific applications by improving their mechanical performance and modifying their barrier and optical properties.

The use of talc particles as filler is a less investigated alternative compared to clay minerals. Talc should be considered a promissory option as polymer reinforcement agent because its world-wide availability, relative low cost, and chemical inertness, as well as,

* Corresponding author. Planta Piloto de Ingeniería Química, PLAPIQUI (UNS-CONICET), Departamento de Ingeniería Química, UNS, Camino La Carrindanga Km. 7, (8000) Bahía Blanca, Argentina. Tel.: +54 0291 4861700.
E-mail address: ovlopez75@yahoo.com.ar (O.V. López).

http://dx.doi.org/10.1016/j.foodhyd.2015.05.030
0268-005X/

its particles have at least one nanometric dimension. This mineral is a naturally occurring magnesium silicate with an ideal chemical formula of $Mg_3Si_4O_{10}(OH)_2$, constituted by stacked platelets, which are formed by thousand of elemental sheets (Steen, 1999). Talc incorporation allows enhancing final properties of starch based materials, without resigning their biodegradable character. Mineral geological origin determines both talc purity, as well as, particle morphology. During talc formation, new mineral phases could be created from preexisting ones. As a consequence, talc ores are also constituted by impurities, including mainly magnesite ($MgCO_3$), calcite ($CaCO_3$), dolomite ($CaMg(CO_3)_2$), and chlorites ($Mg_5(Al,Fe)(Al,Si)_4O_{10}(OH)_8$), among others (Steen, 1999). On the other hand, talc morphology is related to its lamellarity (determined by the individual platelet size) and crystalline character. Thus, long and well-defined platelets are attributed to 'macrocrystalline' talc with high lamellarity. Meanwhile, heterogeneous stack of small and irregular platelets is characteristic of 'microcrystalline' mineral with low lamellarity (Piniazkiewicz, McCarthy, & Genco, 1994). Several works reported that these differential characteristics derived from mineral genesis determine final properties of synthetic composites. Thereby, talc purity affects its efficiency by enhancing composite thermal properties since even low levels of impurities (metal ions) catalyze polymer degradation (Flaris, 2005). Moreover, particle characteristics determine their aggregation tendency, affecting filler distribution and dispersion within polymeric matrix (Pukánszky, 1995). Castillo, Barbosa, and Capiati (2013) reported that macrocrystalline talc lead to improved mechanical properties than microcrystalline one on polypropylene based composites. However, concerning to biopolymer matrixes, there is a lack of studies related to the influence of mineral genesis on composite properties. The relevance of knowing geomorphological characteristics of filler particles, associated to its formation process, resides on the possibility to forecast composite performance and to design materials with specific properties depending on their applications.

The goal of this work was to evaluate the influence of talc morphological characteristics derived from different geological genesis, on TPS bionanocomposite structure. Besides, the effect of filler presence on optical, thermal, barrier, and mechanical properties of thermo-compressed films was also evaluated through several techniques.

2. Materials and methods

2.1. Materials

Native corn starch was provided by Misky-Arcor (Tucumán, Argentine) with an amylose content of 23.9 ± 0.7% (López, García, & Zaritzky, 2008). Talc samples from two different ores were used: Australian talc (A10), with a purity degree of 98% w/w, and Argentinean talc (SJ10), containing up to 16% w/w of impurities. Both samples were kindly supplied by Dolomita SAIC (Argentine). Geological origin induces mineral differences such as purity, crystalline character, and morphological aspects.

As it was reported in a previous work, A10 is a platy talc sample, having particles organized in laminar concentric domains like an "onion" structure (Castillo, Barbosa, & Capiati, 2012). Besides, this talc has a microcrystalline morphology, where small platelets are stacked up heterogeneously. On the other hand, SJ10 is a blocky-type talc sample with long and well stacked up platelets which corresponds to a macrocrystalline structure (Castillo, Barbosa, Maiza, & Capiati, 2011). Moreover, these talc particles appear as blocks, with abrupt and well defined borders. Analytical grade glycerol (Anedra, Argentine) was used as plasticizer.

2.2. Thermoplastic starch mixtures

Mixtures of native corn starch, glycerol (30% w/w), distilled water (45% w/w) and talc nanoparticles (0 and 8.7% w/w) were prepared. Component concentrations were expressed in g per 100 g of starch, which implies that 0 and 5% w/w of talc, respect to TPS, were used. Mixtures were prepared using both A10 and SJ10 talc samples and formulations were named TPS, TPS +5% A10 and TPS +5% SJ10, respectively. Talc was premixed with starch to achieve good particle dispersion between both powders. Then, glycerol and distilled water were added and samples were mixed and conditioned at 25 °C during 24 h. Mixtures were processed in a Brabender Plastograph (Brabender, Germany) at 140 °C and 50 rpm for 15 min.

2.3. Films preparation

Thermoplastic starch films were obtained by thermocompression using an hydraulic press, following the processing conditions reported in a previous work (Castillo, López, et al., 2013). Mixtures were conditioned at 25 °C and 60% relative humidity (RH) and films were prepared at 140 °C and 150 kg cm^{-2} during 6 min. Film thickness was measured at least in ten different locations using a micrometer.

2.4. Microstructural characterization

2.4.1. Scanning Electron Microscopy (SEM)

Talc nanoparticles distribution in TPS matrix, as well as, homogeneity and appearance of the developed films, were examined by SEM. This study was performed in a JEOL JSM-35 CF electron microscope (Japan), with a secondary electron detector. Films were cryofractured by immersion in liquid nitrogen, mounted on bronze stubs and coated with a gold layer (~30 Å), using an argon plasma metallizer (sputter coater PELCO 91000). Thus, film surfaces and their cross-sections were satisfactorily observed.

2.4.2. Transmission electron microscopy (TEM)

Dispersion of talc layers was analyzed by TEM. Samples were microtomed at room temperature using an ultramicrotome LKB Ultrotome 2088 (KB-Produkter AB., Bromma, Sweden) equipped with a diamond knife. Ultrathin sections (~1000 Å) were picked up using a copper grid. Samples were examined using a JEOL 100 CX (JEOL, Japan) operating at an acceleration voltage of 100 kV.

2.4.3. X-ray diffraction (XRD)

Crystal structure identification of thermoplastic starch, crystallinity degree of TPS and talc intercalation/exfoliation were studied by XRD. Diffractograms were obtained in an X-ray diffractometer Philips PW1710 (Philips, Holland), provided with a tube, a copper anode, and a detector operating at 45 KV and 30 mA within 2θ from 3 to 60°. Crystallinity degree (CD) of TPS matrixes were calculated as the ratio between absorption peaks (without considering those corresponding to talc) and the total diffractogram area, expressed as percentage (%). Besides, according to Bragg's equation, basal spacing (d) of talc layers was obtained in order to evaluate the degree of platelets intercalation and exfoliation (Mbey, Hoppe, & Thomas, 2012).

Besides, TPS crystallite size was estimated from XRD spectra, according to the Scherrer equation:

$$L_{hkl} = \frac{K\lambda}{B_{hkl}\cos\theta} \quad (1)$$

where L_{hkl} is the crystallite size in the perpendicular direction to (hkl) reflection plane, K is the crystallite shape factor (0.9), λ is the wavelength of CuK radiation (1.5425 Å), B_{hkl} is the reflection width at the half-maximum intensity, and θ is the Bragg angle of the particular reflection (2θ is the scattering angle).

2.4.4. Fourier Transform Infrared Spectroscopy (FTIR)

Spectra were obtained using a Thermo Nicolet Nexus spectrophotometer (United States). Samples were prepared by mixing thermoplastic starch mixtures as fine powder with KBr (99% Sigma Aldrich, United States) at 3% w/w. The mixture was pressed and a transparent sample was obtained. Spectra were obtained from 100 accumulated scans at 4 cm^{-1} resolution in the range 4000–400 cm^{-1}.

2.5. Thermal properties

A Perkin Elmer Pyris I (United States) calorimeter was used. Approximately 10 mg of film, previously conditioned at 25 °C and 60% RH, were weighted in hermetic pan in order to avoid water loss. An empty hermetic pan was used as reference. Samples were heated from 20 to 250 °C at 10 °C/min, under nitrogen atmosphere. From these thermograms, the following parameters were obtained: onset (T_0) and melting (T_m) temperatures and enthalpy of melting (ΔH_m) associated to this thermal transition.

2.6. Optical properties

2.6.1. Opacity and UV barrier capacity

The absorbance spectrum (200–800 nm) was recorded using an SHIMADZU UV-160 (Japan) spectrophotometer. Films were cut into rectangles (3 × 1 cm) and placed on the internal side of a quartz spectrophotometer cell. The blocking effect of filler to UV transmission was calculated with the equation proposed by Sanchez-Garcia, Hilliou, and Lagaron (2010):

$$\text{Blocking effect} = \frac{\left(\%\,T_{control} - \%\,T_{bionanocomposite}\right)}{m_t} \quad (2)$$

where $\%T_{control}$ and $\%T_{bionanocomposite}$ refer to percent transmittance for the TPS control film and the bionanocomposite film, respectively, and m_t is the percent of talc with respect to starch mass. The blocking effect was calculated at 300 and 700 nm in the UV and visible region, respectively (Mbey et al., 2012).

Film opacity (AU nm) was defined as the area under the recorded curve, determined by an integration procedure according to Piermaría et al. (2011) and the standard test method for haze and luminous transmittance of transparent plastics recommendations (ASTM D1003-00).

2.6.2. Color measurements

Film color determinations were performed using a Hunterlab UltraScan XE (United States) colorimeter in the transmittance mode. Color parameters (L^*, a^*, and b^*) were recorded according to the CIELab scale, in at least ten randomly selected positions for each film sample. Color parameters range from $L^* = 0$ (black) to $L^* = 100$ (white), $-a^*$ (greenness) to $+a^*$ (redness), and $-b^*$ (blueness) to $+ b^*$ (yellowness). Standard values considered were those of the white background ($L^* = 94.42$, $a^* = -0.67$, and $b^* = 0.61$). Besides, ΔL^*, Δa^*, and Δb^* were calculated, taking into account the standard values of the white background, and the parameter color difference was also determined following the equation used by Monedero, Fabra, Talens, and Chiralt (2009):

$$\Delta E = \sqrt{\Delta L^{*2} + \Delta a^{*2} + \Delta b^{*2}} \quad (3)$$

2.7. Water vapor permeability

Water vapor permeability (WVP) was determined according to ASTM F 1249-89 standard method using a PERMATRAN-W® Model 3/33 (Mocon Inc., United States). Film samples, previously conditioned at 25 °C and 60% RH, were placed in a test cell which is divided into two chambers separated by the specimen. The inner chamber is filled with nitrogen (carrier gas) and the outer chamber with water vapor (test gas). Water molecules diffuse through the film to the inside chamber and water vapor transmission rate (WVTR) is registered. Measurements were carried out at 25 °C and films were subjected to a partial water vapor pressure gradient. Masked specimens with precut aluminum foil were used, leaving an uncovered film area of 5 cm^2. From WVTR values, WVP was calculated using Equation (4).

$$WVP = \frac{l\,WVTR}{\Delta p} \quad (4)$$

where l corresponds to film thickness (m) and Δp is the partial pressure difference across the film (Pa).

2.8. Mechanical properties

Tensile tests were performed in an Instron 3369 universal mechanical testing system (Instron, United States) using a crosshead speed of 2 mm/min and a load cell of 50 N. Ten test specimens(13 × 100 mm), previously conditioned at 25 °C and 60% RH, were measured for each film formulation and stress-strain curves were calculated from load–displacement data. Young's modulus (E), maximum tensile strength (σ_m) and elongation at break (ε_b) were calculated according to ASTM D882-00 standard method. Besides, resilience modulus (U_r) and yield strain (ε_y), as well as toughness, were also obtained.

2.9. Statistical analysis

A completely randomized experimental design was used to characterize bionano-composite films. Analysis of variance (ANOVA) was used to compare mean differences of samples properties, imparted by talc morphology. Besides, comparison of mean values was performed by Fisher's least significant difference test conducted at a significance level $p = 0.05$.

3. Results and discussion

3.1. Microstructural characterization

By visual appreciation, composite films based on thermoplastic corn starch containing talc particles presented good appearance, being translucent and easy to handle. However, their microstructural characteristics such as dispersion, distribution, and orientation of particles within TPS, as well as, particle-matrix interfacial adhesion, determine the final properties of the films.

SEM micrographs of composite are presented in Fig. 1. Fracture surface of TPS films was smooth and structurally homogeneous, without cracks presence. According to Zhang, Yu, Xie, Naito, and Kagawa (2007), the occurrence of a continuous matrix texture is a favorable characteristic in order to develop starch films/sheets for coating and packaging applications. As it was expected, since glassy breakage was achieved during films cryofracture, no plastic

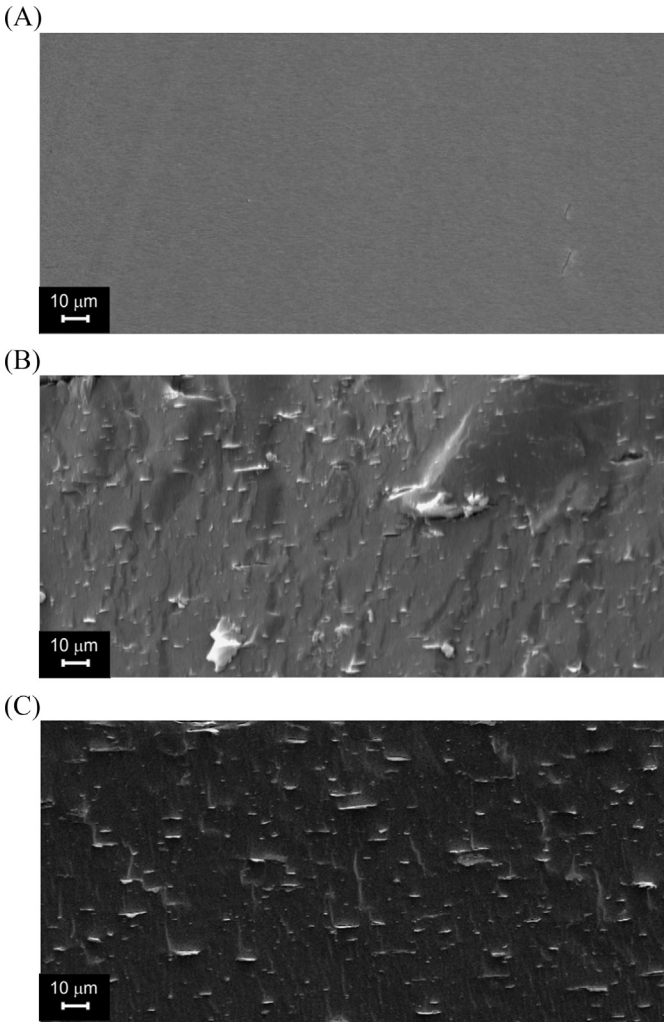

Fig. 1. SEM micrographs of films based on: (A) TPS; (B) and (C) bionanocomposites of TPS with 5% w/w of A10 and SJ10 talc particles, respectively.

deformation was detected. The absence of starch unmelted granules could be the result of a good bionanocomposites processing by melt-mixing and thermo-compression. Effective starch thermoplasticization was achieved since no perpendicular channels to film surface, produced by glycerol migration from the matrix, were observed (López, Zaritzky, Eiras Grossmann, & García, 2013). Films fracture surfaces were analyzed using different magnifications (200, 540, 1000, 2000, and 6000×), and no phase separation was evidenced. SEM micrograph of TPS (Fig. 1A) exhibited similar characteristics of starch films previously reported (Castillo, López, et al., 2013; López, Castillo, García, Villar, & Barbosa, 2015). Fracture surfaces of bionanocomposite films were flat and compact, with talc particles distributed homogeneously along TPS matrix (Fig. 1B and C). Regardless talc morphology, a preferential orientation of particles was evidenced as a consequence of thermo-compression process. Besides, a good particle-matrix adhesion was reached for both talc samples, without observing particle pulling-out phenomenon. Thus, voids absence around particles, which is indicative of a continuous interphase between talc and TPS, could be attributed to the interaction, by hydrogen bonds, between hydrophilic groups on talc edge surface with hydroxyl groups of plasticized starch. Similar results were reported by De Carvalho, Curvelo, and Agnelli (2001) for thermoplastic starch and kaolin composites. Talc crystalline character influenced on bionanocomposites microstructure. Fracture surface corresponding to films containing A10 talc exhibited some aggregates as a consequence of the onion-type structure of these particles (Fig. 1B). On the other hand, in composites with SJ10 talc, the blocky morphology was observed (Fig. 1C). Characterization of both talc particles were previously reported by Castillo et al. (2011).

TEM micrographs corresponding to TPS films containing A10 and SJ10 talc particles are shown in Fig. 2. In both bionanocomposites it was observed an incipient intercalation of talc platelets by TPS matrix, which was indicated with arrows in the corresponding TEM micrographs. Thus, regardless talc morphology, individual platelets that still retained their stacked structure were detected. Similarly, Gao, Dong, Hou, and Zhang (2012) reported a slight intercalated multilayered morphology for starch films with clays having different hydrophobicities.

In order to evaluate structural changes in TPS matrix induced by the addition of talc from different genesis, FTIR study was performed. Fig. 3 shows the spectra of TPS, talc samples, as well as, developed bionanocomposites. As it was reported in a previous work (Castillo, López, et al., 2013), characteristics bands of starch and glycerol functional groups were evidenced in TPS. FTIR spectrum corresponding to A10 and SJ10 talc samples shared the same characteristics bands located at 3676 cm^{-1} (Mg_3—OH), 1018 cm^{-1} (Si—O—Si stretching), 671 cm^{-1} (—OH deformation), 536 and

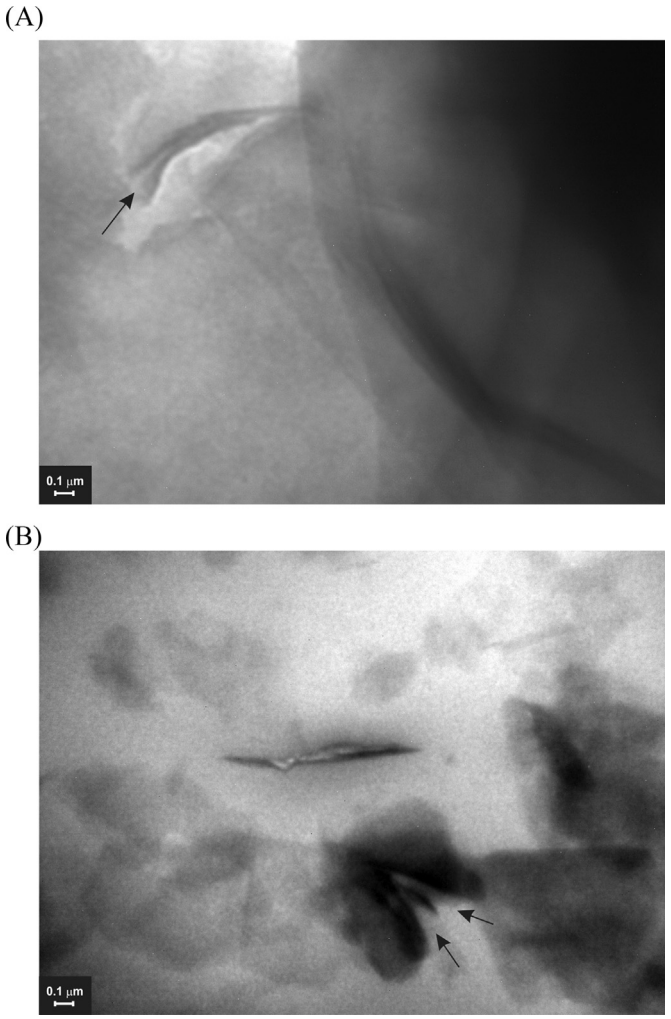

Fig. 2. TEM micrographs of TPS bionanocomposites films with 5% w/w of: (A) A10 and (B) SJ10 talc particles.

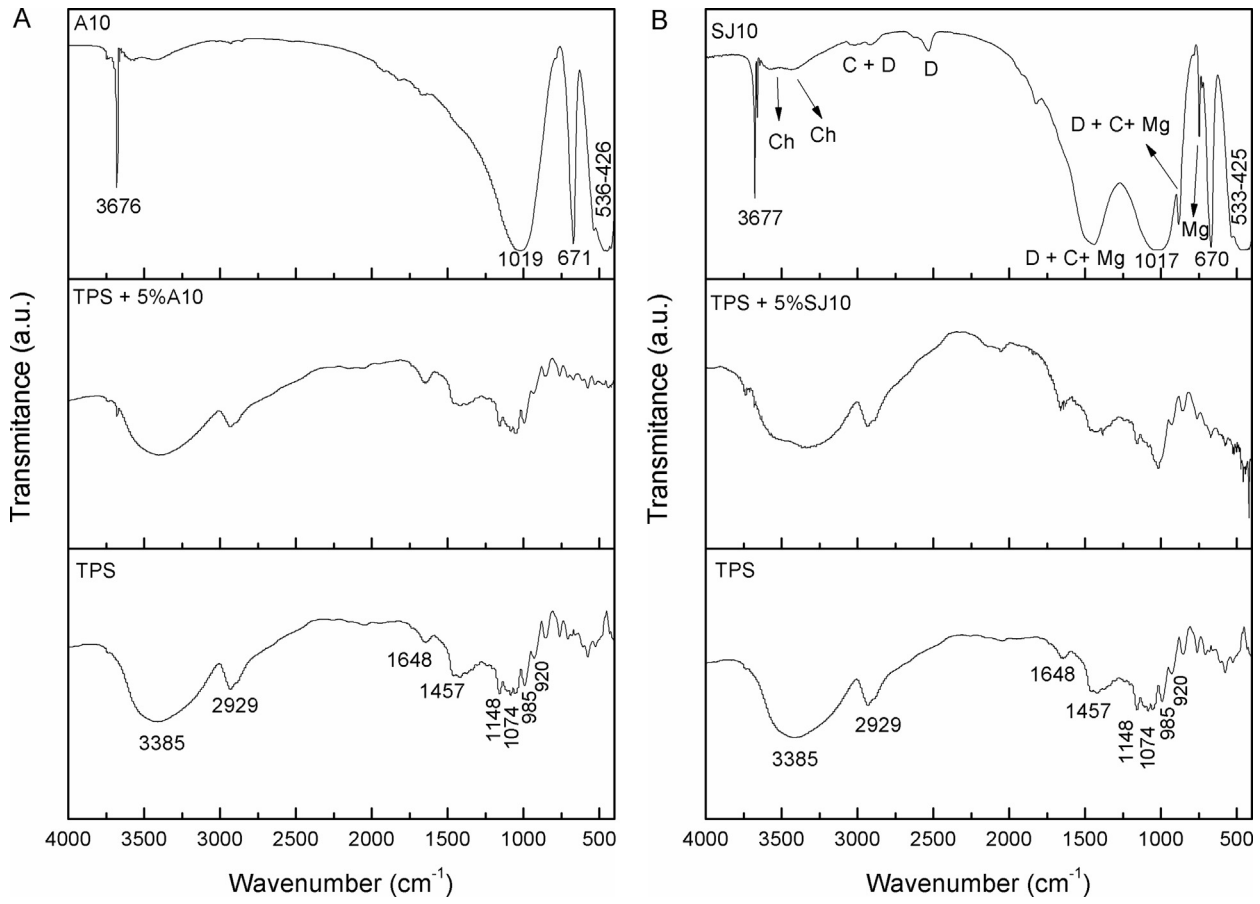

Fig. 3. FTIR spectra of: (A) A10 talc, TPS and bionanocomposites with 5% w/w of A10, (B) SJ10 talc, TPS and bionanocomposites with 5% w/w of SJ10.

452 cm^{-1} (Si–O–Mg), 466 cm^{-1} (Mg–O) and 426 cm^{-1} (Si–O). Similar results were reported by Castillo et al. (2011). Talc genesis is also revealed by the presence of some impurities such as chlorite (Ch), calcite (C), dolomite (D), and magnesite (Mg) in SJ10 sample (Fig. 3B).

Talc presence in both composites was evidenced by detecting typical mineral bands in FTIR spectra (Fig. 3). A proper structural analysis was possible due to good discrimination of talc bands from those corresponding to TPS. In addition, this technique is useful to corroborate actual filler concentration in composite materials (Castillo, Barbosa, et al., 2013). In this work, the concentration was determined through the bands intensity ratio (BIR) between talc (669 cm^{-1}) and TPS (1648 cm^{-1}), at different sections of the specimens. Previously, a calibration curve was built to determine actual filler concentration in both bionanocomposites. Since selected talc band is independent of mineral genesis, it was obtained only one calibration curve for both composites which satisfactorily fitted experimental data ($r^2 = 0.994$). Actual talc concentrations were very close to nominal ones, being 4.95 ± 0.39 and 4.97 ± 0.45 for composites with A10 and SJ10, respectively. In addition, a good level of particles distribution was evidenced since similar bands ratio were obtained among all sections tested for each specimen. This observation is attributed to an efficient melt-mixing process.

Fig. 4 shows XRD spectra corresponding to TPS matrix, A10 and SJ10 talc samples, as well as, TPS composites. In addition, this figure includes degree of crystallinity (CD) values of starch in TPS and bionanocomposites. Plasticized starch pattern corresponded to V-type crystalline structure, which has been described by Castillo, López, et al. (2013). Taking into account that native starch presents an A-type pattern, the lack of reflections corresponding to this crystalline structure could be an indicative of the melt processing efficiency. This observation is in accordance to the absence of "ghosts" or remnant structure of starch granules, observed by SEM. Talc addition did not modify TPS crystalline structure neither matrix CD values, regardless different geological origins of the studied fillers. Impurities of SJ10 talc sample, as a consequence of its formation process, were detected by XRD and they are identified in the spectra using the same nomenclature included in FTIR analysis (Fig. 4B). In addition, XRD studies provide qualitative information concerning to particle intercalation and exfoliation. Intercalation occurs when polymer enters among the filler platelets and increase the interplanar distance (*d*-spacing), but retaining their original stacked structure. On the other hand, when disordered platelets are pushed apart from the stacks, particle exfoliation takes place (McGlashan & Halley, 2003). In order to evaluate the occurrence of these phenomena in the studied composites, talc reflection corresponding to (002) basal plane was considered. This peak for A10 and SJ10 samples appeared at $2\theta = 9.40°$ (*d*-spacing = 9.40 Å) and $2\theta = 9.43°$ (*d*-spacing = 9.37 Å), respectively. Concerning to the corresponding TPS composites with A10 and SJ10, this reflection occurred at $2\theta = 9.47°$ (*d*-spacing = 9.34 Å) and $2\theta = 9.58°$ (*d*-spacing = 9.23 Å), respectively. Comparing *d*-spacing values between talc reflection in natural mineral samples and in the corresponding bionanocomposites, it was not detected a significant change. Partial particle intercalation previously observed in TEM micrographs was not detected by XRD analysis. In addition, a little shift of this diffraction peak toward higher angles was detected.

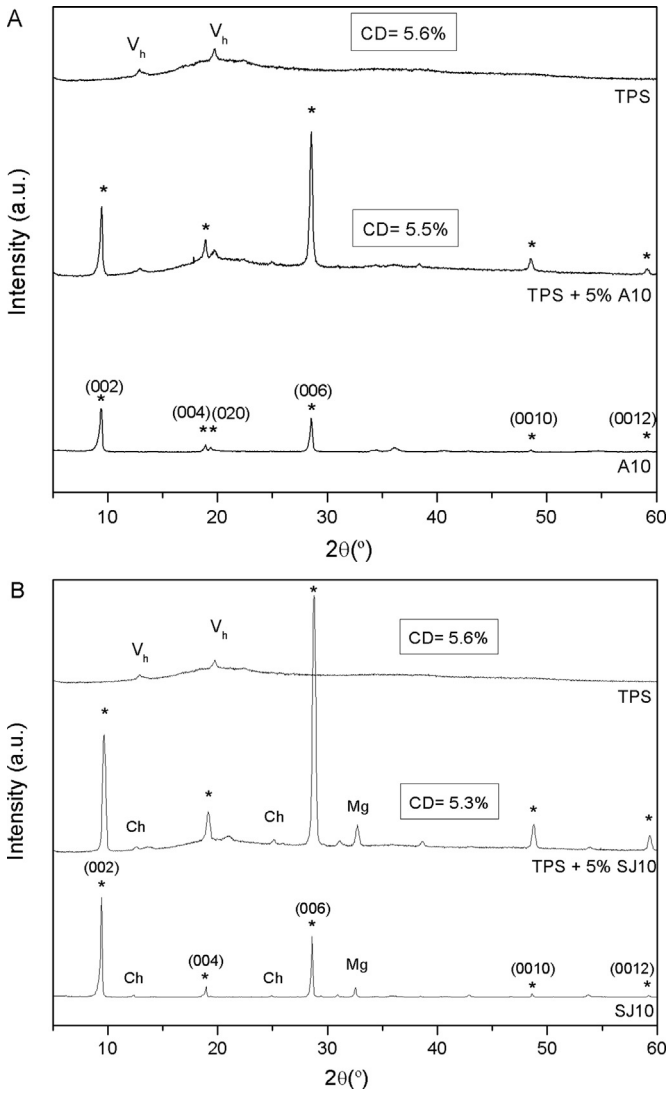

Fig. 4. XRD diffractograms of: (A) A10 talc, TPS and bionanocomposites with 5% w/w of A10, (B) SJ10 talc, TPS and bionanocomposites with 5% w/w of SJ10.

Benetti et al. (2005) reported similar results for composites based on polypropylene containing cloisite. These authors stressed that the lack of particle intercalation could be attributed to thermal and mechanical treatments involved in composites processing. Besides, the fact that talc did not have exchangeable cations in the interplanar distance restricts the possibility of particle exfoliation, as it was previously reported by Castillo, López, et al. (2013).

XRD analysis also provides additional information related to talc morphology influence on TPS crystallites size. This effect was evaluated considering TPS peak located at $2\theta = 12.8°$, since in this spectral zone, matrix reflections do not overlap with those corresponding to talc samples. According to Scherrer equation, starch crystallites size in the perpendicular direction to the considered reflection plane, for TPS and bionanocomposites with A10 and SJ10 were 45, 23, and 28 nm, respectively. These results could be attributed to talc presence, which induce the formation of smaller TPS crystallites than those detected for pure starch plasticized matrix. Similar tendency were reported for different composites, such as for synthetic materials based on poly-propylene containing talc particles (Castillo et al., 2012).

Processing conditions of composites based on a semicrystalline polymer are established by thermal properties of the thermoplastic matrix. Particularly, in the case of plasticized starch materials, the most relevant thermal parameters are those involved in the matrix melting process. Thermograms of TPS, as well as, those corresponding to bionano-composites presented one endothermic transition related to starch matrix melting since talc particles decompose at temperatures higher than 1000 °C. Temperature range (20–250 °C) was chosen in order to assure a complete melting of TPS matrix. Preliminary measurements were performed to study crystallization behavior of these composites but the obtained results suggested that polymeric matrix suffered degradation after melting process. Thermal properties of the developed films are included in Table 1. The fact that talc addition shifted TPS onset and melting temperatures to lower values could be attributed to the presence of smaller starch crystallites. These results are in agreement with those obtained by XRD analysis. Besides, this observation could be a consequence of talc nucleating capability on TPS crystallization, as it was previously reported by other authors (Castillo, Barbosa, et al., 2013; Pukánszky, 1995). Concerning to melting enthalpy, even though talc addition decreased this thermal parameter, its reduction was not significant (Table 1). High dispersion of the obtained results could be related to samples heterogeneity, as it was previously reported (Castillo, López, et al., 2013). Regarding to the influence of talc morphology on thermal properties, it can be observed that composites containing A10 presented lower onset and melting temperatures than those formulations with SJ10. This behavior could be based on A10 platy morphology, inducing the formation of starch crystallites with reduced dimensions. Thus, A10 talc presence led to a higher shift of T_o and T_m of TPS matrix than SJ10 (Table 1), in agreement with TPS crystallites sizes determined from aforementioned XRD data.

3.2. Optical properties

As it is well-known, films optical properties define their feasible applications, especially in packaging field. Table 2 shows particles blocking effect, as well as, opacity and UV barrier capacity of TPS-talc composite films. Influence of filler presence on matrix absorption capacity at different spectral regions can be quantified through particle blocking effect. Concerning to SJ10 particles, this optical property was 2.7 and 3.4 times higher than the corresponding to A10 for 300 and 700 nm, respectively. These results lead to a noticeable influence of particle morphology of talc samples on film optical properties. In this sense, SJ10 blocky morphology provides to TPS based films a more effective physical barrier against UV and visible radiation than A10 platy one.

Other relevant films characteristic is their opacity. Filler presence increased significantly this property, corroborating their visual appreciation. Composites based on TPS with SJ10 resulted two times more opaque than those with A10. Another package functional property is UV barrier capacity, especially for those products which can be deteriorated by this kind of radiation, such as lipid oxidation. Starch based materials were able to absorb UV light, presenting an absorption peak between 270 and 300 nm. Talc addition increased this property, being more notorious for bionanocomposites containing SJ10 particles (Table 2). In this sense, films based on TPS with SJ10 presented a UV barrier capacity 190% higher than those with A10 talc.

Table 3 shows color parameters of TPS films developed in this study. A10 talc presence did not affect luminosity of starch based films. However, the incorporation of SJ10 particles induced a slight reduction in L^* values of TPS, associated to talc macrocrystalline character. Concerning to chromaticity parameters, both talc samples led to a significant reduction in a^* values, meanwhile they increased b^* measurements of composite films. This tendency was more evident in films containing SJ10 talc, attributed not only to its

Table 1
Thermal properties of thermoplastic corn starch films (TPS) with A10 and SJ10 talc particles.

Film formulation	Onset temperature (°C)	Melting temperature (°C)	Melting enthalpy (J/g TPS)
TPS	133.1 ± 1.3[a]	156.4 ± 2.1[a]	140.7 ± 32.2[a]
TPS + 5% A10	127.8 ± 3.1[b]	144.3 ± 0.8[b]	115.8 ± 17.3[a]
TPS + 5% SJ10	131.8 ± 2.0[a,b]	147.3 ± 0.1[c]	114.4 ± 23.1[a]

Reported values correspond to the mean ± standard deviation. Values within each column followed by different letters indicate significant differences ($p < 0.05$).

Table 2
Blocking effect values of mineral particles. Opacity and UV absorption peak area of thermoplastic corn starch films (TPS) with A10 and SJ10 talc.

Film formulation	Blocking effect		Opacity (AU × nm)	UV absorption peak area (AU × nm)
	300 nm	700 nm		
TPS	–	–	31.8 ± 6.4[a]	17.1 ± 1.4[a]
TPS+5%A10	0.027 ± 0.001[a]	0.038 ± 0.002[a]	109.0 ± 9.3[b]	24.8 ± 1.2[b]
TPS+5%SJ10	0.072 ± 0.005[b]	0.129 ± 0.021[b]	233.1 ± 0.2[c]	46.6 ± 3.3[c]

Reported values correspond to the mean ± standard deviation. Values within each column followed by different letters indicate significant differences ($p < 0.05$).

Table 3
Color parameters of thermoplastic corn starch films (TPS) with A10 and SJ10 talc particles.

Film formulation	Color parameters			
	L* (Luminosity)	a* (green-red)	b* (blue-yellow)	ΔE
TPS	90.9 ± 0.1[a]	−0.77 ± 0.03[a]	2.32 ± 0.18[a]	3.93 ± 0.15[a]
TPS+5%A10	91.0 ± 0.1[a]	−0.39 ± 0.01[b]	4.01 ± 0.10[b]	4.82 ± 0.12[b]
TPS+5%SJ10	89.9 ± 0.0[b]	−0.13 ± 0.02[c]	5.45 ± 0.04[c]	6.61 ± 0.04[c]

Reported values correspond to the mean ± standard deviation. Values within each column followed by different letters indicate significant differences ($p < 0.05$).

macrocrystalline character but also to the presence of impurities. Higher ΔE values of composite films are mainly attributed to the increment of yellowness by talc addition.

3.3. Water vapor permeability (WVP)

One of the main purpose of incorporating mineral particles as filler in a polymer matrix is to tailor their barrier properties for specific applications. Regarding to TPS materials, starch hydrophilic character is the responsible of their high WVP. Thus, this intrinsic characteristic conditions starch materials uses, especially in food packaging. In this sense, filler addition to TPS films is focused on the decrease of transmission rate of water vapor flow through the matrix. Talc influence on WVP of TPS films is shown in Fig. 5. As it could be observed, talc presence led to a significant decrease in WVP values of TPS films, regardless mineral genesis. This reduction could be attributed to several contributions. First, particles laminar morphology and thermo-compression process allowed preferential spatial disposition of the filler within the matrix, as it could be observed by SEM (Fig. 1). This orientation, where particles are aligned and parallel to film surface, leads to a tortuous path for gas/vapor flow. Other reasons that justifies WVP reduction by talc presence could be attributed to that TPS hydroxyl groups are engaged by hydrogen bonds with talc hydrophilic sites on mineral edge surfaces. In addition, WVP is reduced since water vapor flow is repelled by talc basal surfaces which are hydrophobic. Likewise,

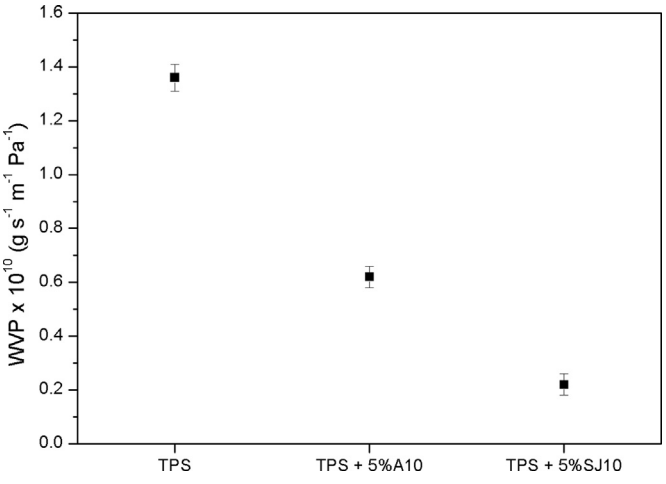

Fig. 5. Influence of A10 and SJ10 talc addition (5% w/w) on water vapor permeability (WVP) of TPS films.

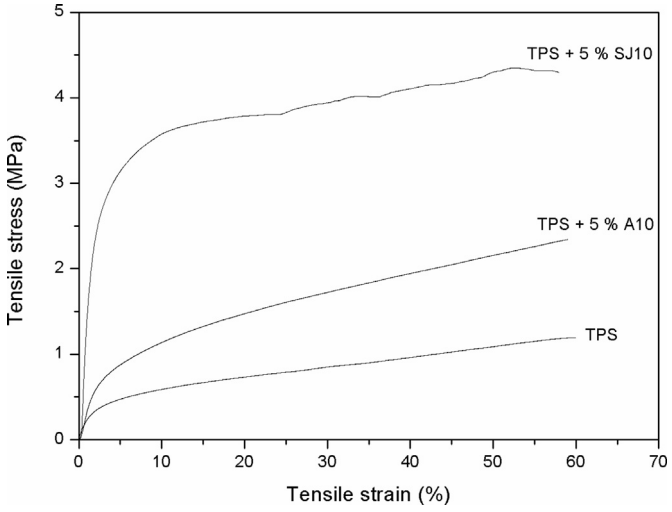

Fig. 6. Stress-strain curves of films based on TPS and bioananocomposites with 5% w/w of A10 and SJ10 talc particles.

Table 4
Mechanical properties of thermoplastic corn starch films (TPS) with A10 and SJ10 talc particles.

Film formulation	Young's Modulus (MPa)	Maximum tensile strength (MPa)	Elongation at break (%)
TPS	22.7 ± 1.7[a]	1.19 ± 0.04[a]	62.2 ± 4.1[a]
TPS + 5% A10	38.2 ± 3.0[b]	2.34 ± 0.04[b]	59.0 ± 1.1[a]
TPS + 5% SJ10	266.9 ± 47.3[c]	4.04 ± 0.40[c]	55.3 ± 5.4[a]

Reported values correspond to the mean ± standard deviation. Values within each column followed by different letters indicate significant differences ($p < 0.05$).

macrocrystalline character of SJ10 talc induced a higher WVP reduction (~85%) than A10 microcrystalline one, which decreased this property up to 55%. Despite the low talc concentration used, a significantly WVP reduction was achieved, widening starch based materials application fields. Moreover, the possibility of tailoring TPS barrier properties is a powerful tool to design materials with specific functionalities by the incorporation of different fillers at several concentrations.

3.4. Mechanical properties

Addition of filler particles to starch materials has another relevant goal in order to improve their mechanical performance plus tailoring final barrier properties. Fig. 6 shows tensile test curves corresponding to TPS and composites with talc particles. As it could be observed, talc addition did not modify stress-strain behavior of TPS films. Under tensile assays conditions, these materials resulted ductile since their fracture strain were higher than 5% (Callister, 2003). Slight stepped increment detected in stress values from 25% strain up to film breakage in composites with SJ10 talc, could be related to mineral morphology which offers a higher tensile resistance than A10 particles. Mechanical properties corresponding to developed starch based films are presented in Table 4. As it was expected, talc incorporation increased elastic modulus, as well as, tensile strength of TPS ($p < 0.05$). Composites with SJ10 talc presented elastic modulus and tensile strength values 7 and 1.7 times, respectively, higher than those with A10 particles. Concerning to elongation at break, it was observed that talc incorporation did not modify this mechanical property, regardless mineral genesis (Table 4). Talc addition influence on TPS mechanical properties could be explained through amphiphilic character of particles which induces two different interactions with starch matrix. Hydrophilic edge surface of particles are able to form hydrogen bonds with starch chains. On the other hand, physical interactions occur between hydrophobic basal surface of talc and starch plasticized matrix. TPS reinforcement by talc addition is mainly associated to the localized and strong interaction between the mineral edge surface and the TPS matrix. Elastic modulus increment by talc addition revealed higher interatomic bonding forces between particles and matrix than those corresponding to starch–starch and starch–glycerol interactions. The further strengthening of TPS achieved by SJ10 addition could be associated mainly to two factors. First, the aforementioned particles morphology of this mineral sample which allows accommodating more starch chains on edge talc surfaces than A10, giving a higher tensile resistance than TPS. On the other hand, interfacial adhesion between SJ10 and TPS seems to be better than the corresponding with A10. This improved adhesion would allow effective load transference from starch matrix to talc particles, increasing composite maximum tensile stress. Conversely, in the case of composites elongation at break, which quantifies their ductility, the major contribution could be attributed to a poor interfacial adhesion between basal talc surface and TPS. This weak interaction would allow starch chains orientation with tensile axis and their sliding during the assays, leading to hold TPS films ductility.

4. Conclusions

Films bionanocomposites based on thermoplastic corn starch containing talc particles with different morphology were obtained by melt-mixing and thermo-compression.

Films cross-sections were structurally homogeneous, without pores and cracks. Regardless talc crystalline character, particles were well-distributed with a distinctive orientation, showing a good compatibility with TPS matrix. An incipient intercalation of talc platelets by plasticized starch was evidenced in the composites. Also, differential particle morphology between both talc samples was observed by SEM. TPS crystalline structure was not affected by the presence of particles, regardless mineral morphology. Talc addition shifted TPS onset and melting temperatures to lower values due to the presence of smaller starch crystallites, in accordance with XRD results. Even though, both talc samples increased visible and UV barrier capacity of TPS films, macrocrystalline character of SJ10 particles induced the major changes in this optical property. Besides, talc addition modified luminosity and chromaticity parameters of TPS films. Talc presence affected starch films barrier properties, decreasing their WVP values. Blocky morphology of SJ10 particles induced the highest reduction of this barrier property. Although, talc incorporation increased the amount of rigid phase in bionanocomposites, TPS stress-strain behavior was not affected. However, the presence of particles within the matrix acted as a reinforcement agent since they induced an increase in tensile strength values. In addition, bionanocomposites presented a higher resistance to elastic deformation than TPS films, being more evident for films with SJ10 particles. Regardless talc crystalline character, elongation at break was not affected.

Even though, both talc samples have similar behavior, there is a significant influence of crystalline character, induced by their geological origin, on TPS final properties. However, macrocrystalline talc seems to be more effective in order to enhance UV and water vapor barrier capacity, as well as, mechanical properties of TPS films.

Acknowledgments

Authors gratefully acknowledge the financial support provided by Consejo Nacional de Investigaciones Científicas y Técnicas (CONICET, Argentina) (grant no. PIP0428) and the Universidad Nacional del Sur (UNS, Argentina) (grant no. PGI 24/M135).

References

Benetti, E., Causin, V., Marega, C., Marigo, A., Ferrara, G., Ferraro, A., et al. (2005). Morphological and structural characterization of polypropylene based nanocomposites. *Polymer, 48*, 8275–8285.

Bodirlau, R., Teaca, C., & Spiridon, I. (2013). Influence of natural fillers on the properties of starch-based biocomposite films. *Composites Part B: Engineering, 44*, 575–583.

Callister, W. (2003). *Materials science and engineering. An introduction* (6th ed.). W. USA: John Wiley & Sons, INC.

Castillo, L., Barbosa, S., & Capiati, N. (2012). Influence of talc genesis and particle surface on the crystallization kinetics of polypropylene/talc composites. *Journal of Applied Polymer Science, 126*, 1763–1772.

Castillo, L., Barbosa, S., & Capiati, N. (2013). Influence of talc morphology on the mechanical properties of talc filled polypropylene. *Journal of Polymer Research, 20*, 152–160.
Castillo, L., Barbosa, S., Maiza, P., & Capiati, N. (2011). Surface modifications of talcs. Effects of inorganic and organic acid treatments. *Journal of Materials Science, 46*, 2578–2586.
Castillo, L., López, O., López, C., Zaritzky, N., García, M. A., Barbosa, S., et al. (2013). Thermoplastic starch films reinforced with talc nanoparticles. *Carbohydrate Polymers, 95*, 664–674.
Chung, Y., Ansari, S., Estevez, L., Hayrapetyan, S., Giannelis, E., & Lai, H. (2010). Preparation and properties of biodegradable starch–clay nanocomposites. *Carbohydrate Polymers, 79*, 391–396.
De Carvalho, A., Curvelo, A., & Agnelli, J. (2001). A first insight on composites of thermoplastic starch and kaolin. *Carbohydrate Polymers, 45*, 189–194.
De Melo, C., Garcia, P., Eiras Grossmann, M., Yamashita, F., Dall'Antônia, L., & Mali, S. (2011). Properties of extruded xanthan-starch-clay nanocomposite films. *Brazilian Archives of Biology and Technology, 54*, 1223–1233.
Flaris, V. (2005). Talc. In M. Xanthos (Ed.), *Functional fillers for plastics* (pp. 207–220). Weinheim, Germany: Whiley-VCH.
Gao, W., Dong, H., Hou, H., & Zhang, H. (2012). Effects of clays with various hydrophilicities on properties of starch–clay nanocomposites by film blowing. *Carbohydrate Polymers, 88*, 321–328.
López, O., García, M., & Zaritzky, N. (2008). Film forming capacity of chemically modified corn starches. *Carbohydrate Polymers, 73*, 573–581.
López, O., Zaritzky, N., Eiras Grossmann, M., & García, M. (2013). Acetylated and native corn starch blend films produced by blown extrusion. *Journal of Food Engineering, 116*, 286–297.
López, O., Castillo, L., García, M., Villar, M., & Barbosa, S. (2015). Food packaging bags based on thermoplastic corn starch reinforced with talc nanoparticles. *Food Hydrocolloids, 43*, 18–24.
Lu, Y., Weng, L., & Cao, X. (2005). Biocomposites of plasticized starch reinforced with cellulose crystallites from cottonseed linter. *Macromolecular Bioscience, 5*, 1101–1107.
Ma, X., Chang, P., Yu, J., & Stumborg, M. (2009). Properties of biodegradable citric acid-modified granular starch/thermoplastic pea starch composites. *Carbohydrate Polymers, 75*, 1–8.
Mbey, J., Hoppe, S., & Thomas, F. (2012). Cassava starch–kaolinite composite film. Effect of clay content and clay modification on film properties. *Carbohydrate Polymers, 88*, 213–222.
McGlashan, S., & Halley, P. (2003). Preparation and characterization of biodegradable starch-based nanocomposite materials. *Polymer International, 52*, 1767–1773.
Monedero, F., Fabra, M., Talens, P., & Chiralt, A. (2009). Effect of oleic acid–beeswax mixtures on mechanical, optical and water barrier properties of soy protein isolate based films. *Journal of Food Engineering, 91*, 509–515.
Narkchamnan, S., & Sakdaronnarong, C. (2013). Thermo-molded biocomposite from cassava starch, natural fibers and lignin associated by laccase-mediator system. *Carbohydrate Polymers, 96*, 109–117.
Parra, D., Tadini, C., Ponce, P., & Lugäo, A. (2004). Mechanical properties and water vapor transmission in some blends of cassava starch edible films. *Carbohydrate Polymers, 58*, 475–481.
Piermaría, J., Bosch, A., Pinotti, A., Yantorno, O., García, M., & Abraham, A. (2011). Kefiran films plasticized with sugars and polyols: water vapor barrier and mechanical properties in relation to their microstructure analyzed by ATR/FT-IR spectroscopy. *Food Hydrocolloids, 25*, 1261–1269.
Piniazkiewicz, R., McCarthy, E., & Genco, N. (1994). Talc. In D. Carr (Ed.), *Industrial mineral and rocks* (pp. 1049–1069). Colorado: CME.
Pinto, C., Carbajal, G., Wypych, A., Ramos, L., & Satyanarayana, K. (2009). Studies of the effect of molding pressure and incorporation of sugarcane bagasse fibers on the structure and properties of polyhydroxybutyrate. *Composites Part A. Applied Science and Manufacturing, 40*, 573–582.
Pukánszky, B. (1995).). In *Particulate filled polypropilene: Structure and properties. Polypropilene. Structure, blends and composites* (Vol. 3, pp. 1–70). London: Chapman & Hall. University Press.
Saiah, R., Gattin, R., & Sreekumar, P. (2012). Properties and biodegradation nature of thermoplastic starch, thermoplastic elastomers. In A. El-Sonbati (Ed.), *InTech* (pp. 57–78).
Sanchez-Garcia, M., Hilliou, L., & Lagaron, J. (2010). Nanobiocomposites of carrageenan, zein, and mica of interest in food packaging and coating applications. *Journal of Agricultural and Food Chemistry, 58*, 6884–6894.
Steen, W. (1999). Talc in polypropylene. In H. Karian (Ed.), *Handbook of polypropylene and polypropylene composites* (pp. 237–262). United States: Wiley-VCH.
Tapia Blácido, D., Sobral, P., & Menegalli, F. (2005). Development and characterization of biofilms based on Amaranth flour (Amaranthus caudatus). *Journal of Food Engineering, 67*, 215–223.
Zhang, Q., Yu, Z., Xie, X., Naito, K., & Kagawa, Y. (2007). Preparation and crystalline morphology of biodegradable starch/clay nanocomposites. *Polymer, 48*, 7193–7200.